




REGULAR ARTICLE

Textured Bifacial Silicon Solar Cells Under Various Illumination Conditions

R. Aliev¹, M. Komilov¹, N. Mirzaalimov¹, A. Mirzaalimov², S. Alive³, I. Gulomova^{1,*} , J. Gulomov²

¹ Andijan State University, 170100 Andijan, Uzbekistan

² Andijan State Pedagogical Institute, 170100 Andijan, Uzbekistan

³ Andijan Machine Building Institute, 170100 Andijan, Uzbekistan

(Received 25 June 2024; revised manuscript received 20 October 2024; published online 30 October 2024)

On a sunny day, the front side of the bifacial solar cells is illuminated with direct and the rear side with the diffused light. Therefore, it is important to study the effect of diffusion and direct light on the bifacial solar cell. In this study, the effects of diffuse and direct light and temperature on the textured bifacial solar cell were determined by simulation. According to the obtained results, the optimal value of the angle of base of texture for a bifacial silicon solar cell is 580. On a cloudy day, under diffuse light illumination on both sides, the planar and optimally textured solar cells have an efficiency of 13.14% and 16.03% and a short-circuit current of 4.34 mA/cm² and 5.49 mA/cm². The short-circuit current is 2.28 mA/cm² and 2.88 mA/cm² when only front side is illuminated with diffuse light. On a sunny day, when direct light falls on the front side and diffuse light falls on the rear side, the short-circuit current of the planar and optimally textured solar cell are 27.79 mA/cm² and 35.16 mA/cm², respectively. Short-circuit current are 25.73 mA/cm² and 32.65 mA/cm² when only front side illuminated with direct light.

Keywords: Silicon solar cell, Texture, Diffuse light, Direct light.

DOI: [10.21272/jnep.16\(5\).05025](https://doi.org/10.21272/jnep.16(5).05025)

PACS numbers: 85.60.Bt, 78.20.Bh, 84.60.Jt

1. INTRODUCTION

Today, the use of renewable energy sources to meet energy needs is becoming urgent. Among renewable energy sources, solar energy makes up a large share. Solar cells are mainly used to convert solar energy into electricity. Currently, electricity from solar cells accounts for 4.5% of the world's electricity [1].

Increasing the efficiency of solar cells and reducing their cost is one of the main tasks of today. So far, the maximum efficiency of solar cell has reached 39.5% [2]. In industry, 96% of solar cells are made of silicon [3]. Because silicon is one of the most common materials on earth. The efficiency of the silicon-based solar cell is 29% according to the Shockley-Quizzer theory [4] and in the experiment [5] is equal to 26.8%. The optimal thickness of a silicon-based solar cell in the industry is 175 μm [6]. To further reduce the cost of the solar cell, it is better to use materials with a high absorption coefficient in thin layers. One such material is perovskite [7]. Perovskite solar cells are very easy to synthesize [8] and the efficiency is higher than that of silicon-based solar cells [9]. But their stability is very low, so they are not produced at an industrial level [10]. Since almost all solar cell manufacturing plants are silicon-based, scientists are interested in creating silicon-based tandem solar cells [11].

There are mainly 3 types of losses in solar cells [12]:

optical, electrical and thermal. Optical losses include the reflection of light from the surface [13], parasitic absorption [14], spectral mismatches [15] is included. To reduce the amount of light reflected from the surface 2, SiO₂, a SiN_x, MgF₂, and TiO₂ optical layers [16] and textures are created [17]. When the texture is created, the depth of light absorption is also reduced, which allows to reduce the thickness of the solar cell. Spectral mismatch is eliminated by forming tandem structures of various semiconductors in order of decreasing band gap [18]. According to the theory, the efficiency of a tandem solar cell with an infinite layer can reach 68.7% [19]. Tandem structures also prevent parasitic absorption. Because high-energy photons are absorbed in a layer with a large band gap, it is more likely that high-energy electrons will reach the contacts without thermalization. In addition, the spectral mismatch was also reduced by introducing metal nanoparticles in the n region of the solar cell [20]. A nanoparticle absorbs infrared light and emits light in the visible range, that is, it modifies the light spectrum [21]. Therefore, the spectrum of light absorbed by the solar cell expands. To reduce the amount of recombination in solar cells, the front and rear sides are covered with passivating materials [22]. Because the surface of the solar cell becomes active due to dangling bonds, the recombination rate is high. When the solar cell heats up, the efficiency and the open circuit voltage

* Correspondence e-mail: irodakhon.gulomova@yahoo.com



decrease sharply [23]. Many cooling designs have been recommended to prevent overheating [24].

The sunlight falling on the solar panel is mainly divided into two spectrums: direct and diffuse. Diffuse light is formed due to the scattering of sunlight in air molecules and its return from the ground [25]. Industrially produced solar cells are mainly single-sided sensitive and the rear side is covered with a solid metal contact. By making the rear contact in the form of a grid and covering it with an optical layer, a bifacial solar cell can be formed. Since infrared rays are mainly absorbed by metal contacts, the thermal properties of the solar cell can be improved by making the rear contact in the form of a grid. In addition, direct light mainly falls on the front side of the solar cell, and diffuse light falls on the rear side. That is, there is an opportunity to convert diffused light into electricity. Also, there is not much difference between the cost of single-sided and bifacial solar cells. Hence, it is important to research and optimize bifacial solar cells. Therefore, in this scientific work, a bifacial textured solar cell was investigated using simulation for geometric optimization.

The article is structured as follows: method, results and discussion, and conclusion. The method section describes the steps of bifacial solar cell simulation and their theoretical basis in detail. In the result and discussion section, the results obtained through simulation are scientifically proved, and it is divided into four parts: Optimal texture, planar and textured bifacial solar cells, and the effect of diffuse light.

2. MATERIALS AND METHODS

2.1 Device Simulation Procedure

Four tools of the Sentaurus TCAD program were used to study the bifacial solar cell [26]: Sentaurus Device, Sentaurus Structure Editor, Sentaurus Visual or Sentaurus Workbench.

In the Sentaurus Structure Editor, take the bifacial solar cell shown in Fig. 1 and create a geometric model of the system for making the same illumination for both sides. To create a geometric model in Sentaurus Structure Editor, code is written in Tool Command Language (TCL). Took the sun cell and used the loop operator to create the textures on the both sides. To provide the same intensity of light to the front and rear sides, a silver reflector with an angle 90° was installed on the bottom of the solar cell. A rectangular silver reflector has a hypotenuse of $2L$ and a height of L . L is the width of the solar cell. The light falling on the open surface of width L is directed perpendicularly to the rear side of the solar cell with the help of a silver reflector.

Direct AM1.5 and diffusion AM1.5 spectrum were chosen as the light source. To passivate the front and rear sides of the solar cell and reduce the reflection coefficient, both side is covered with 100 nm thick SiO_2 . The thickness of the emitter and base regions is $1 \mu\text{m}$ and $18.35 \mu\text{m}$, respectively. Its width is $20 \mu\text{m}$. Phosphorus atoms with $1 \text{E}17 \text{cm}^{-3}$ and Boron atoms with $1 \text{E}15 \text{cm}^{-3}$ are doped to emitter and base regions, respectively. 200 nm thick highly doped n++

($1 \text{E}18 \text{cm}^{-3}$) on the top of the emitter and p^{++} ($1 \text{E}16 \text{cm}^{-3}$) layers on the bottom of the base were formed to ensure good transport of electrons and holes to the contacts. Textures were created on the front and rear sides at the same time. The width of the textures is $1 \mu\text{m}$ and it was not changed during the study. Texture height is changed from $0.1 \mu\text{m}$ to $1.9 \mu\text{m}$ in $0.1 \mu\text{m}$ increments to change the texture-based angle. Also, the case where the height of the texture is $0 \mu\text{m}$ was considered as a planar solar cell. The system was meshed in 2 different sizes in order to increase the calculation efficiency and achieve convergence. First, all regions were meshed with the same $0.5 \mu\text{m}$ size in the x and y directions. The p-n junction, contact, and highly doped areas were meshed in the x and y directions at a finer size of $0.05 \mu\text{m}$ and $0.01 \mu\text{m}$, respectively.

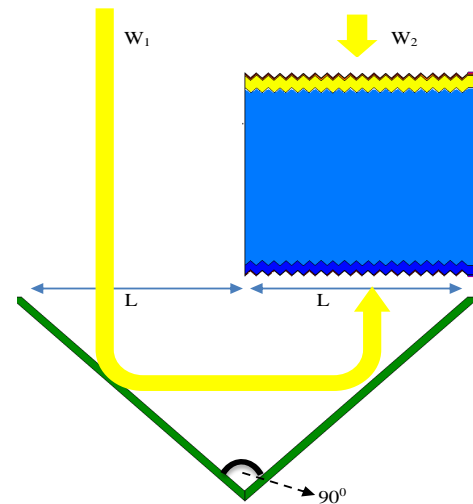


Fig. 1 – A geometric model designed to illuminate the front and rear sides of a textured solar cell

The necessary physical parameters of the materials used in simulation in Sentaurus Device were given. As silver is ideal, its reflection coefficient is taken as 1. Through this, the rear and front areas of the solar cell were illuminated with the same intensity of light. In this work, the solar cell was illuminated in 3 different positions: front, rear and both sides. For this, 2 virtual light windows w_1 and w_2 were created on Sentaurus Device (Fig. 1). Light was cast onto window w_2 for front illumination only, and window w_1 for backlight illumination only. For equal illumination of the front and back, w_1 and w_2 were illuminated at the same time.

2.2 Theoretical Background of Device Simulation

From a theoretical point of view, simulation of solar cells can be divided into 2 phases: optical and electrical. Transfer Matrix Method [27], Beam Propagation [28] via Ray Tracing [29] methods are widely used for Optical Simulation. In this study, the Ray Tracing method was used to determine the optical properties of the solar cell. Because the refraction of light between the textures and the refraction of the light from the silver reflectors and

falling on the rear of the solar cell can be taken into account in the Ray Tracing method. The optical boundary conditions between the solar cell and the air are determined using Fresnel coefficients given in Eq. 1 [30].

$$\begin{cases} r_i = \frac{n_1 \cos \beta - n_2 \cos \gamma}{n_1 \cos \beta + n_2 \cos \gamma} \\ t_i = \frac{2n_1 \cos \beta}{n_1 \cos \beta + n_2 \cos \gamma} \\ r_p = \frac{n_1 \cos \gamma - n_2 \cos \beta}{n_1 \cos \gamma + n_2 \cos \beta} \\ t_p = \frac{2n_1 \cos \beta}{n_2 \cos \beta + n_1 \cos \gamma} \end{cases} \quad (1)$$

Here: r_i go t_i Fresnel coefficients for a transversely polarized electromagnetic wave, r_p go t_p Fresnel coefficients for a parallel polarized electromagnetic wave, β is the angle of incidence of the light beam.

As an optical boundary condition between air and the silver reflector, the reflection coefficient was set to 100%. In this case, absorption and transmission of light in the reflector was prevented.

Light is absorbed when it passes through a solar cell. In Ray Tracing, 50,000 rays were fall on the solar cell. When each ray passes through the solar cell, its energy is reduced, that is, part of the energy is absorbed by the solar cell. The absorbed part of the energy is calculated by Burger Lambert's law. The number of photons in the beam can be determined by dividing the energy of the beam by the energy of the photon in the corresponding spectrum. Not all absorbed photons form electron-hole pairs. The energy of each photon is checked using the quantum yield function. If the photon energy is greater than the band gap, it is absorbed and forms an electron-hole pair. The resulting excitons are separated due to the internal electric field created by the p-n junction. That is, electrons and holes are affected by the internal electric field in different directions. The internal electric field and potential generated in the solar cell are calculated using Poisson's equation given in Eq. 2 [31].

$$\Delta\varphi = -\frac{q}{\varepsilon}(p - n - N_D + N_A) \quad (2)$$

Here: ε is the dielectric constant, n and p are the concentration of electrons and holes, N_D and N_A - concentration of donor and acceptors, q - electron charge.

Electrons and holes also move due to the concentration difference, and this is called diffusion movement. The transport of electrons and holes caused by the difference in concentrations and internal electric field is calculated using drift-diffusion model given in Eq. 3 [32].

$$\begin{aligned} \vec{J}_n &= \mu_n(n\nabla E_C - 1.5nkT\nabla \ln m_n) + D_n(\nabla n - n\nabla \ln \gamma_n) \\ \vec{J}_p &= \mu_p(p\nabla E_V + 1.5pkT\nabla \ln m_p) - D_p(\nabla p - p\nabla \ln \gamma_p) \end{aligned} \quad (3)$$

Here: J_n and J_p are current density generated by

electrons and holes, m_n and m_p are effective mass of electrons and holes, g_n and γ_p are quantities determined using the Fermi function, D_n and D_p are electron and hole diffusion coefficient, μ_n and μ_p mobility of electrons and holes.

This research mainly researched silicon-based solar cell. A silicon-based solar cell has a large proportion of Shockley-Read-Hall (SRH) and Auger recombination. The portion of radiative recombination is almost less than 1%. Because silicon has the indirect band structure. Therefore, only SRH and Auger recombination in silicon were considered in the model. SRH recombination occurs due to defects, and its rate mainly depends on the doping concentrations and defects. SRH is calculated for cases with 1-level, 2-level and n-level defects. In the simplest case, it was calculated using Eq. 4 for level 1 [33].

$$R_{net}^{SRH} = \frac{np - \gamma_n \gamma_p n_{i,eff}^2}{\tau_p (n + \gamma_n n_1) + \tau_n (p + \gamma_p p_1)} \quad (4)$$

Here: n - concentration of electrons, p - concentration of holes, g_n , c_p - coefficients, t_n , t_p - lifetime of electrons and holes, n_1 , p_1 - concentration of electrons and holes in an energy level caused by a defect.

Auger recombination mainly depends on the concentration of charge carriers. There is a big difference in the concentration of charge carriers formed in a solar cell when only one side is illuminated and when both sides are illuminated. When both sides are illuminated, the concentration of charge carriers increases, which means that the rate of Auger recombination also increases. Therefore, Auger recombination can play a key role in changing the parameters of the solar cell. Eq. 5 was used to calculate Auger recombination [34].

$$R_{net}^A = (C_n n + C_p p)(np - n_{i,eff}^2) \quad (5)$$

Here: n - concentration of electrons, p - concentration of holes, C_n , C_p - Auger coefficients. $n_{i,eff}$ - effective specific charge carrier concentration.

Charge carriers are accumulated in the contacts and create a potential difference. The potential between the metal contact and silicon was calculated using the ohm-ic boundary condition given in Eq. 6.

$$\begin{aligned} \varphi &= \varphi_F + \frac{kT}{q} \operatorname{sinh} \left(\frac{N_D - N_A}{2n_{i,eff}} \right) \\ n_0 p_0 &= n_{i,eff}^2 \\ n_0 &= \sqrt{\frac{(N_D - N_A)^2}{4} + n_{i,eff}^2} + \frac{N_D - N_A}{2} \\ p_0 &= \sqrt{\frac{(N_D - N_A)^2}{4} + n_{i,eff}^2} - \frac{N_D - N_A}{2} \end{aligned} \quad (6)$$

Here: $n_{i,eff}$ - concentration of effective intrinsic charge carriers, φ_F is the Fermi potential at the contact.

3. RESULT AND DISCUSSION

3.1 Optimal Texture

There are 2 optimal ways to reduce the reflection coefficient of a solar cell: coating with anti-reflection layers and creating textures on the surface. In this work, 100 nm thick SiO₂ is created on the front and rear surfaces of a silicon-based solar cell based on literature analysis [35]. The width of the texture on the front and rear surfaces was kept unchanged at 1 μm, and only the height was changed from 0.1 μm to 1.9 μm. Fig. 2 shows the dependence of the short-circuit current of a bifacial solar cell on the height of the pyramid. When both sides of the solar cell are equally illuminated, when the height of the pyramid changes from 0.1 μm to 0.5 μm, the short-circuit current is sharply increased to 6.75 mA/cm², between 0.5 – 0.8 μm height is a little increased to 0.97 mA/cm² and between 0.8 – 1.9 μm height is decreased to 2.78 mA/cm². When only front side is illuminated, the short-circuit current is increased to 0.43 mA/cm² in the height range of 0.1 – 0.3 μm², increased to 4.76 mA/cm² in the range of 0.3 – 0.5 μm², increased to 0.49 mA/cm² in the range of 0.5 – 0.8 μm and almost decreased linearly to 1.37 mA/cm² in the range of 0.8 – 1.9 μm. The reason for the short-circuit current changing at different rate in different intervals of the texture height is the increase in the number of refractions of the light in the intervals of the pyramid. When only the rear surface is illuminated, unlike when the front and both sides are illuminated, it was found that there are 2 extremums in the dependence function of the short-circuit current on the height of the pyramid. That is, the short-circuit current is increased to 0.8 mA/cm² in the pyramid height of 0.1 – 0.2 μm, decreased to 0.61 mA/cm² in the range of 0.2 – 0.4 μm, also again increased to 1.69 mA/cm² in the height range of 0.4 – 0.8 μm, and as in the front and both sides illuminated case it is de-creased linearly to 0.31 mA/cm² in the range of 0.8 – 1.9 μm.

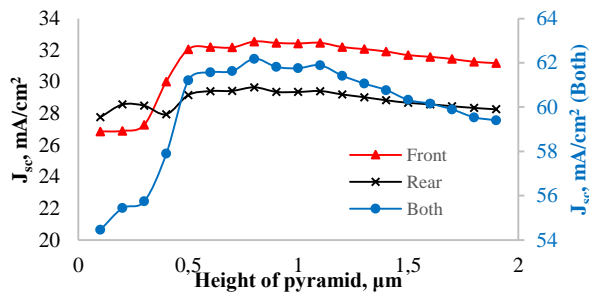


Fig. 2 – Dependence of the short-circuit current on the height of the pyramid of the solar cell with the front and rear sides textured under front, rear and both side illumination

Fig. 2 shows the short-circuit current as a function of the height of the pyramid, in all illumination conditions which is front, rear and both sides, the short-circuit current reached a maximum value at 0.8 μm of the texture height, and they were 32.54 mA/cm², 29.64 mA/cm², 62.18 mA/cm², respectively. In Guan’s study [36], it was found that the short-circuit current of a double-sided textured silicon-based solar cell with front

side illumination is 37.71 mA/cm². When the height of the texture increases, the photon absorption depth decreases, which causes the solar cell to reduce the reflection coefficient and absorb more photons in the volume. Therefore, the short-circuit current increased when the height of the texture increased. A texture height of 0.8 μm can be considered as a critical value for equalization of absorption coefficient and surface recombination depending on the texture height. Fig. 3 shows the dependence of the solar cell open circuit voltage on the texture height in the front, rear and both sides illuminated cases. When the rear and both sides were illuminated, the open circuit voltage changed almost the same, that is, it decreased by leaps and bounds. But only in the front-lit state, the open circuit voltage reached its maximum value at the value of 0.4 μm of the height.

The open circuit voltage mainly depends on the p-n and material properties, so when the height of the texture increases, the open circuit voltage changes almost by a small amount. When increasing the concentration of charge carriers, the bandgap of silicon narrows, so the open circuit voltage is also reduced. Fig. 4 depicts the dependence of the fill factor on the texture height in front, back, and side-illuminated conditions of a silicon-based solar cell.

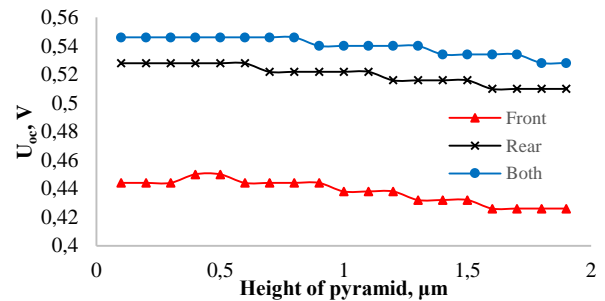


Fig. 3 – Dependence of the open circuit voltage on the height of the pyramid of the textured solar cell under front, rear and both side illumination

The fill factor also decreased as a function of texture height for all three cases. As the texture height increases, the active surface of the solar cell increases. This causes an increase in the amount of surface recombination. The fill factor is reduced as the texture height increases, as it reflects the quality of the surface.

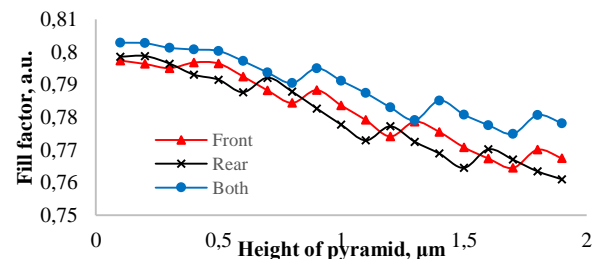


Fig. 4 – The dependence of the fill factor on the height of the pyramid of textured solar cell under front, rear and both side illumination

To evaluate the overall quality of the solar cell, the fill factor is mainly used. Fig. 5 shows the dependence of the solar cell efficiency on the texture height. If we consider the light intensity as a constant value, the efficiency depends only on the current density and voltage. Since the rate of change of the open circuit voltage (Fig. 3) depending on the height of the texture is lower than that of the short circuit (Fig. 2), the function of the efficiency depending on the height of the texture is qualitatively similar to that of the short circuit. From the point of view of the efficiency, the optimal height of the texture was determined to be $0.8 \mu\text{m}$. Considering that we take the texture as an equilateral triangle with a 2D cross-section and a fixed base of $1 \mu\text{m}$, the base angle of the optimal texture is 58° . In our previous studies, the optimal value of the base angle of the texture formed on the surface of a standard silicon-based solar cell was 70.4° [37]. In Mrazkova's study [38], it was determined that the optimal angle of the base of the texture is 70.59° . In the previous study, a simple one-sided sensitive solar cell was studied, in this study, SiO_2 coated bifacial solar cell was investigated. So, SiO_2 affected the optimal value of the texture. Baker-Finch's [39], the base angle of the (111) silicon-based solar cell when the surface is treated with acid, it was determined that the textures are formed with $50 - 52^\circ$ angles. So, structure which we proposed can be created in the experiment.

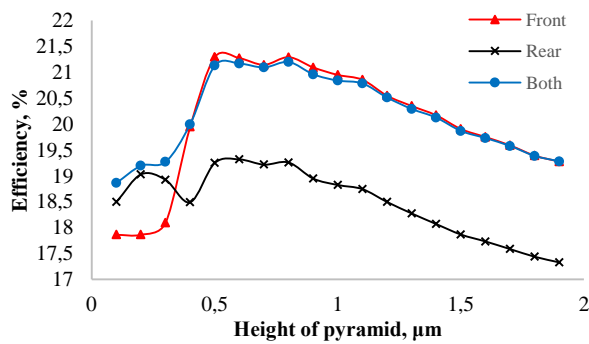


Fig. 5 – Dependence of the efficiency on the height of the pyramid of the textured solar cell under front, rear and both side illumination

3.2 Bifacial Solar Cell with Planar and Optimal Texture

In this section, the photoelectric parameters of the optimally textured and planar solar cell are compared in front, back, and double-side illumination conditions. Fig. 6 shows the I-V characteristics of the front-, back-, and both side-illuminated planar (a) and optimally textured solar cells. In almost all cases, the quality of the functional curvature of the I-V characteristics is the same. The quality of the curve of the I-V characteristic is mainly affected by the series resistance and the parallel resistance. So, the series and parallel resistances did not change significantly when light fall on the front, rear and both sides.

A solar cell can be compared qualitatively based on the I-V characteristic, but not quantitatively. Therefore, using

the I-V characteristics depicted in Fig. 6, the photoelectric parameters listed in Table 1 were determined. The open circuit voltage of the planar and textured solar cell changed by almost the same amount under different illumination conditions. The fill factor also decreased for the planar and textured solar cell in the order of front, back, and both side illumination conditions. However, the fill factor of the planar solar cell was higher in all lighting conditions. Because the solar cell is textured, its active surface increases, so surface recombination increases. Since the fill factor indicates the quality of the surface, it is negatively affected by the increase in surface recombination. The highest fill factor of 79.96% was achieved by the planar solar cell under rear side illumination. Because the input atom concentration in the emitter region and the base region is 100 times different. Surface recombination is also a type of Shockley-Read-Hall (SRH) recombination that depends on the input concentration. Therefore, the activity of the front surface where the emitter is located, that is, the amount of surface recombination, is higher than the rear surface.

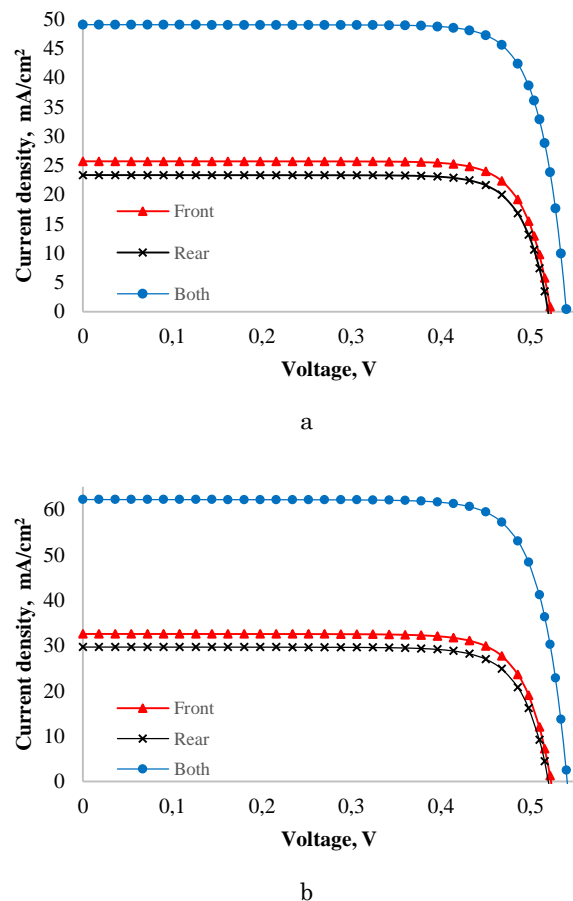


Fig. 6 – I-V characteristics of a planar (a), and optimally textured (b) solar cell under front, rear and both sides illumination

Table 1 – Photoelectric parameters of planar and optimally textured solar cells under front, rear and both side illumination conditions

	Front		Rear		Both	
	Planar	Texture	Planar	Texture	Planar	Texture
J_{sc} , mA/cm ²	25.73	32.54	23.38	29.64	49.06	62.18
U_{oc} , V	0.528	0.528	0.522	0.522	0.546	0.546
FF, %	79.55	78.44	79.96	78.78	79.83	79.05
η , %	17.07	21.29	15.42	19.26	16.89	21.20

When rear side is illuminated, the main charge carriers are formed in the area near the rear surface, and when front-illuminated, they are mainly formed in the areas near the emitter. Therefore, the probability of recombination of electron holes due to surface recombination during rear side illumination is lower than in the case of front side illumination. Therefore, the rear side illuminated planar solar cell had the highest fill factor, and the front-illuminated textured solar cell achieved the lowest fill factor of 78.44%. The highest efficiency was 21.29% for the textured solar cell under front side illumination and the lowest efficiency was 15.42% for the planar solar cell under rear side illumination. The efficiency of the textured solar cell under front and rear side illumination is 21.29% and 19.26%. Ohtsuka's [40], it was determined that the efficiency of silicon solar cell under front and rear side illumination was equal to 21.3% and 19.8%.

Naturally, the short-circuit current of both solar cells increased in the order of rear, front, and side illumination. The double-side illuminated textured solar cell has reached a maximum of 62.18 mA/cm² short circuit current. Fig. 7 shows the distribution of absorbed photons in an optimally textured solar cell with front (a), rear (b) and both sides (c) illumination. During front illumination, photons were mainly absorbed in the area near the *p-n* junction area, and in the rear area, photons were absorbed mainly in the area near the rear surface. Also, the maximum value of the concentration of absorbed photons is $9.17 \text{ E}21 \text{ cm}^{-3}$ when the front side is illuminated and $3.37 \text{ E}21 \text{ cm}^{-3}$ when back side is illuminated.

Due to this, depending on the type and concentration of the input atom, the width of the bandgap of silicon narrows. According to the Jain Roulston model, band gap of the emitter region is smaller than that of the base. In simulation according to the quantum yield function, only photons whose energy is greater than the energy of the bandgap is absorbed in silicon. Decreasing the band gap causes more photons to be absorbed. Therefore, the short-circuit from front-side illumination was higher than that from rear-side illumination. When both sides are illuminated, the maximum absorbed photon concentration is $1.46 \text{ E}22 \text{ cm}^{-3}$. Because the flow of photons emitted from the front side also reaches the rear side of the solar cell, and the flow of photons emitted from the rear side also reaches the front side. That is, in the concentration of photons absorbed in the front, there is a contribution of the flow of photons emitted from the front and rear, as well as in the distribution of absorbed photons in the rear.

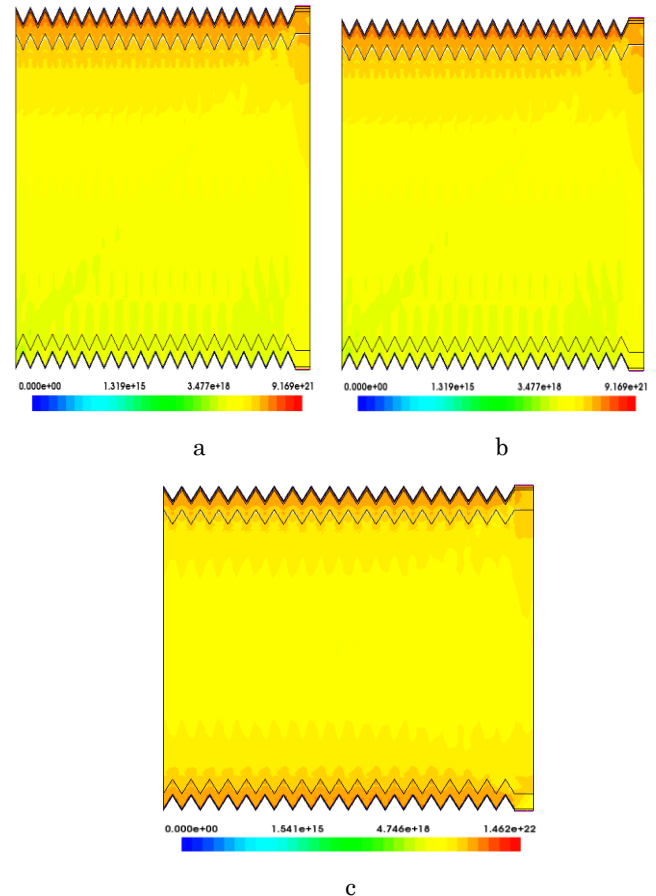
**Fig. 7** – Distribution of absorbed photons in a pyramidal textured solar cell with $0.8 \mu\text{m}$ high and $1 \mu\text{m}$ wide under front (a), rear (b) and both (c) side illumination

Fig. 8 shows the 1D *Y*-axis distribution of absorbed photons planar and textured solar cell under a front, back, and both side illumination. Because, in the model, light falls on the solar cells along the *Y*-axis. In a planar solar cell, the distribution of absorbed photons is linearly exponential in all cases. But the non-linear exponential in the textured solar cell. Because when the light falls perpendicular to the surface of the planar solar cell, it crosses the solar cell along the *Y*-axis and is absorbed along the way. In a textured solar cell, light refracts several times as it hits the texture. In almost all cases, the distribution of absorbed photons in the textured solar cell was higher than that of the planar solar cell, so the short-circuit current of the textured solar cell was also higher than that of the planar one.

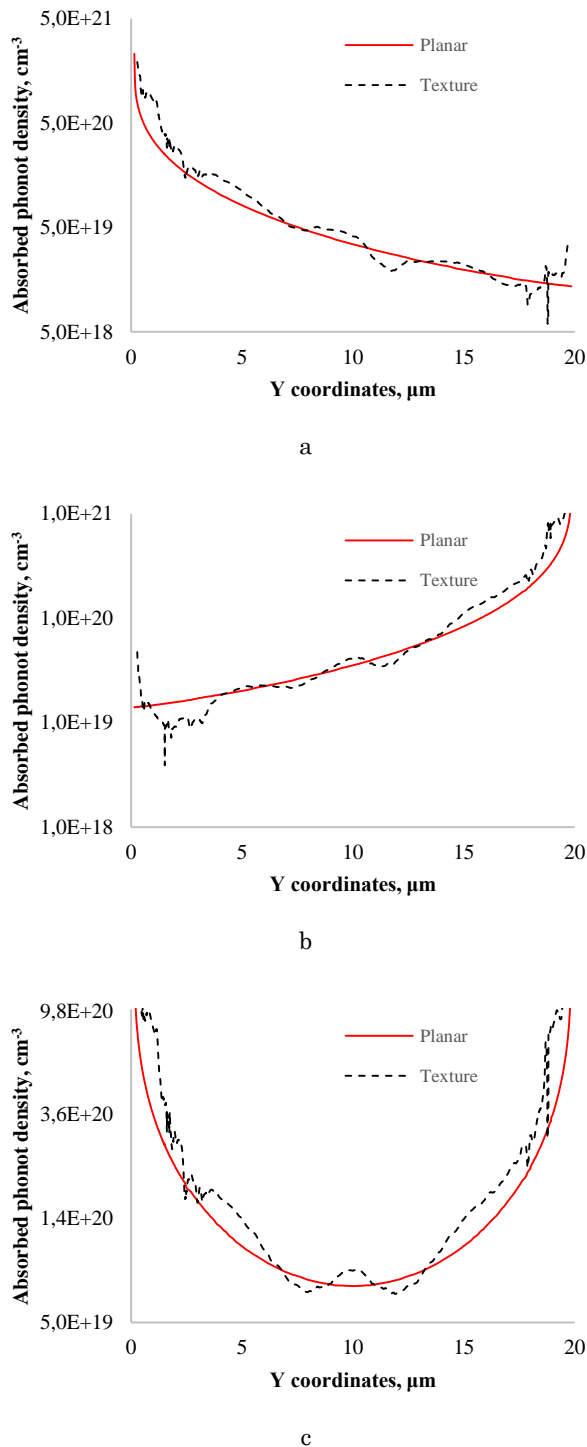


Fig. 8 – 1D distribution of absorbed photons along Y-axis in planar and optimal pyramidal textured solar cells under front (a), rear (b) and both (c) side illumination conditions

Only in areas with low concentration of photon absorption, the absorption in the planar solar cell was higher. But since its share in the total concentration of absorbed photons is very small, it has almost no effect on the short-

circuit current. Electron-hole pairs formed in the solar cell are separated due to the strengthening of the internal electric field and move towards the contacts. Fig. 9 depicts the internal electric field strength in a planar and textured solar cell illuminated on both sides as a function of the Y-axis. In a textured solar cell, the electric field strength penetrates deeper into the core area. This increases the probability of separation of the electron-hole pair formed in the base and reaching the contact. This is another proof that the short-circuit current of the textured solar cell is higher than that of the planar one.

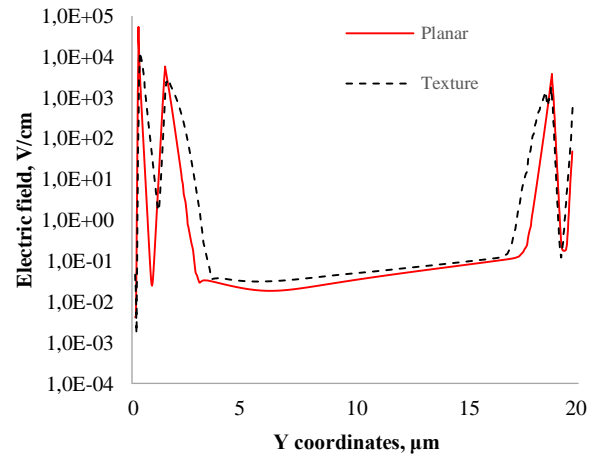


Fig. 9 – Electric field strength distribution of planar and optimally textured solar cell under both side illuminations

Due to the internal electric field, a part of the separated electrons and holes are recombined during their movement towards the contacts. Since silicon is an indirect semiconductor, the percentage of radioactive recombination in it is less than 1%. Therefore, only SRH and Auger recombination are considered in the simulation. Since SRH recombination is mainly caused by defects, it is directly dependent on the input concentration. Increasing the concentration of charge carriers affects Auger recombination. Therefore, the distribution of SRH recombination is not given in this work. Fig. 10 shows the distribution of Auger recombination along the Y-axis in a planar and textured solar cell with front, back, and both sides illuminated. It was found that the amount of Auger recombination in the base region of the planar solar cell in front and both sides is illuminated is higher than that of the textured solar cell. Auger recombination directly depends on the concentration of charge carriers, and according to Fig. 8, the amount of photons absorbed in the base is small in the textured solar cell, so the amount of Auger recombination is also small in the base.

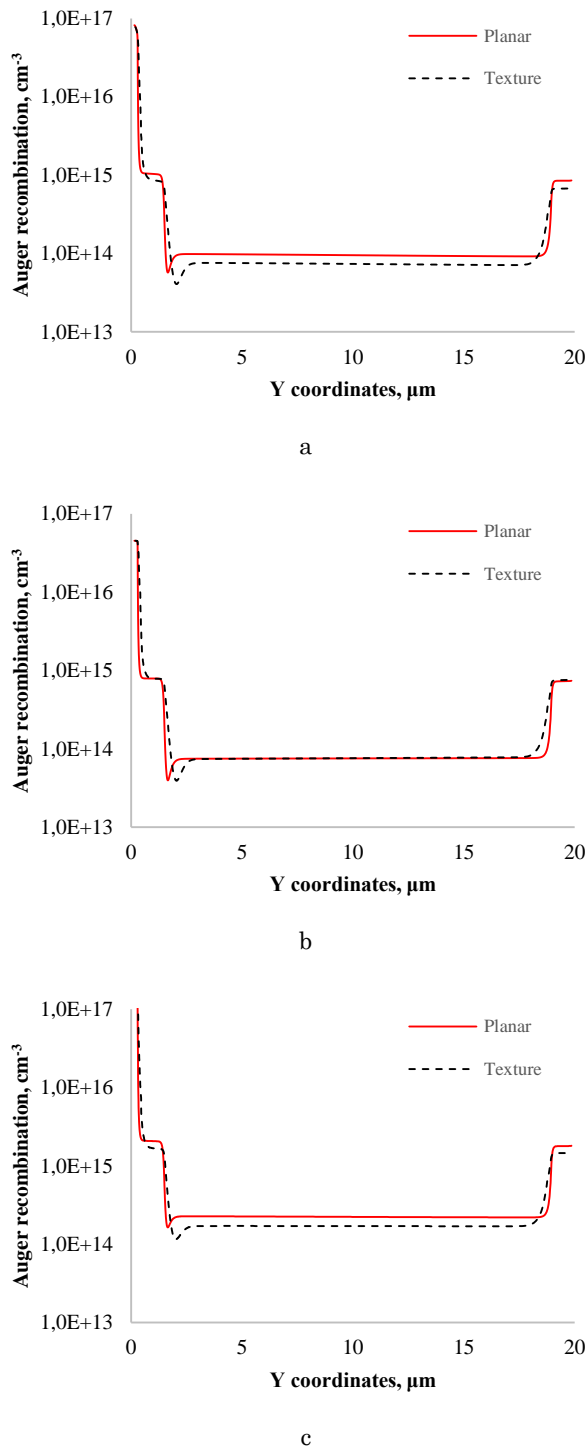


Fig. 10 – 1D distribution of Auger recombination along Y axis in planar and optimal pyramidal textured solar cells under front (a), rear (b) and both (c) side illumination conditions

3.3 Effect of Diffuse Light

In real conditions, direct light falls on the front side of the sun and diffuse light on the rear side. In addition, on

cloudy days, only diffuse light falls on the front and rear sides of the solar cell. Therefore, in this section, the effect of diffuse light on the properties of the solar cell was studied. Fig. 10 shows the AM1.5 spectrum of direct and diffuse light. The intensity of diffuse light is almost 11 times smaller than the intensity of direct light. Because diffuse light is mainly caused by the scattering of sunlight in air molecules and its return from the earth's surface.

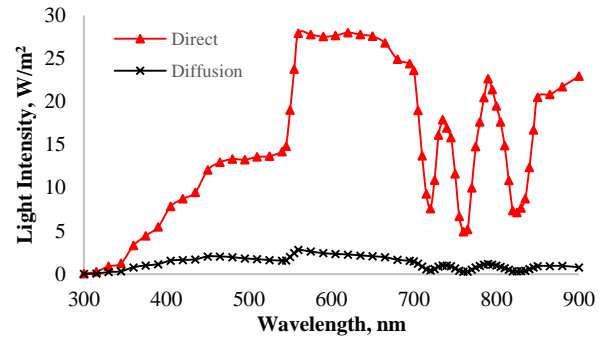


Fig. 11 – Direct and diffuse AM1.5 light spectrum

Fig. 12 shows the *I-V* characteristics of a planar and optimally textured solar cell under diffuse illumination. *I-V* characteristics in the both side illuminated with diffusion light can be considered the *I-V* characteristics of a planar and textured solar cell on a cloudy day. The *I-V* characteristics of planar and textured solar cells under diffuse and direct light (Fig. 12) are qualitatively almost the same.

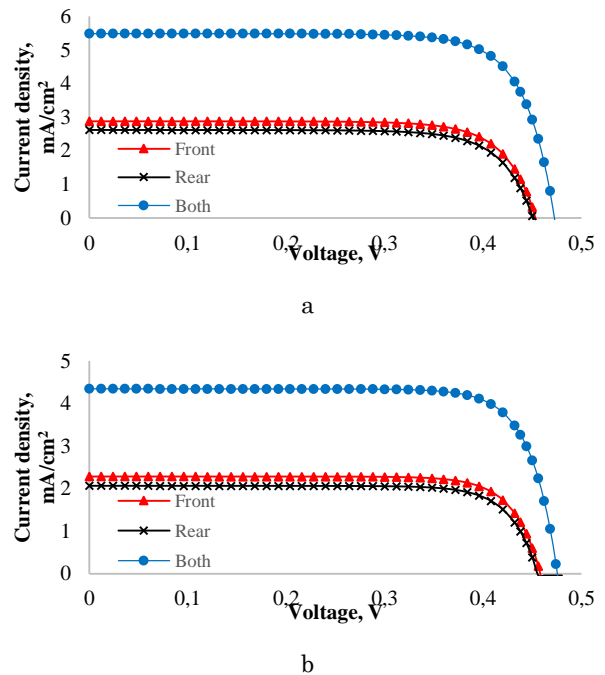


Fig. 12 – *I-V* characteristics of optimally textured (a) and planar (b) solar cells under front, rear and both side illumination

In order to compare the solar cells quantitatively under different radiation, it is necessary to determine their photoelectric parameters. Table 2 lists the photoelectric parameters of the planar and textured solar cells determined using the I-V characteristics in Fig. 2. The dependence of the maximum and minimum values of the photoelectric parameters on the type of solar cell and the method of illumination is the same as in the case of direct light illumination. The short-circuit current of the planar solar cell illuminated by diffuse light is 11.29, 11.35, and 11.30 times lower when illuminated from the rear and both sides, respectively, than when illuminated by direct light. The short circuit current of the textured solar cell was 11.30, 11.31 and 11.33 times less. The open circuit voltage of the planar solar cell was 1.14 times lower and that of the textured solar cell 1.16 times lower in almost all lighting conditions. The short-circuit current varies almost linearly with the light intensity, but the open circuit voltage does not. Because the short-circuit current mainly depends on the concentration of absorbed photons in the solar cell, while the open circuit voltage depends on the material properties. When the solar cell is illuminated, its resistance changes. So, the relative resistance of silicon in a solar cell directly depends on the light intensity. When the light intensity increases, the relative resistance decreases. When the illumination is changed from direct light to diffuse light, the resistivity

of the silicon in the solar cell increases, causing the total internal resistance of the solar cell to increase. Therefore, the open circuit voltage is reduced. The fill factor decreased by an average of 1.65% in the planar solar cell and by an average of 3.48% in the textured solar cell. The fill factor is a quantity strongly related to surface recombination and the concentration of absorbed photons. Since the active surface of a textured solar cell is larger than that of a planar solar cell, the amount of surface recombination is proportional to the surface area. Therefore, the fill factor of the textured solar cell is 2% lower than that of the planar solar cell. The efficiency of the planar solar cell when illuminated with diffuse light was 1.29 times lower than when illuminated with direct light in all illumination conditions. The efficiency of the textured solar cell was 1.34 times lower. Even in this case, the reduction of the efficiency in the textured solar cell to a larger value can be explained by the difference between the surface recombination. The last two columns of Table 2 can be taken as the photoelectric parameters of the planar and textured bifacial solar cell on a cloudy day. The short-circuit current in the case where both sides were illuminated by diffusion light was 1.9 times higher than the short-circuit current in the case where only the front was illuminated. In Pal's [41] work, it was found that the output power of a bifacial solar cell is 20.1-68.1% higher than that of a traditional solar cell.

Table 2 – Photoelectric parameters of planar and optimally textured solar cells under front, rear and both sides diffused light illumination

	Front		Rear		Both	
	Planar	Texture	Planar	Texture	Planar	Texture
$J_{sc}, \text{mA/cm}^2$	2.28	2.88	2.06	2.62	4.34	5.49
U_{oc}, V	0.462	0.456	0.456	0.456	0.48	0.474
FF, %	77.78	75.07	78.16	74.35	78.21	76.41
η, %	13.22	15.88	11.86	14.29	13.14	16.03

Using the photoelectric parameters obtained for diffuse and direct light illumination, it is possible to determine the characteristics of a bifacial solar cell on a sunny day. As a sunny day, it can be considered that the two-way sensitive solar cell is receiving diffused light on the front side and diffused light on the rear side. It was found that the short-circuit current in the state of illumination of both sides is equal to the sum of the short-circuit current in the state of illumination of the front and rear sides. Therefore, the short-circuit current of a bifacial solar cell on a sunny day can be obtained as the sum of the short-circuit currents when the front side is illuminated by direct light and the rear side is illuminated by diffuse light.

4. CONCLUSION

In this paper, a bifacial solar cell was investigated. The front and rear sides of the bifacial solar cell are covered with the same size textures. The optimal value of the angle of base of textures is 580. The effect of diffusion and direct light on a planar and optimally

textured solar cell was studied.

According to the obtained results, the highest efficiency belongs to the optimally textured solar cell with frontal illumination only. Studying the effect of direct and diffuse light on planar and optimally textured solar cells made it possible to theoretically describe a bifacial solar cell in cloudy and sunny conditions. The optimally textured bifacial solar cell produces almost 1.9 times more current than the single-sided sensitive solar cell on a cloudy day and 1.08 times more current on a sunny day.

During this restriction, it was assumed that the influence of the optical layer on the optimal angle of the texture. In further research, it is desirable to study the effect of different optical materials on the properties of the textured bifacial solar cell.

ACKNOWLEDGEMENTS

Authors are grateful to the team of Renewable Energy Source Laboratory for assisting to complete this work.

REFERENCES

- Renewable electricity capacity additions by technology and segment, 2016-2028 – Charts – Data & Statistics – IEA (2024).
- R.M. France, J.F. Geisz, T. Song, W. Olavarria, M. Young, A. Kibbler, M.A. Steiner, *Joule* **6** No 5, 1121 (2022).
- Renewables 2023 – Analysis – IEA (2023).
- A.R. Zanatta, *Results in Optics* **9**, 100320 (2022).
- M.A. Green, E.D. Dunlop, M. Yoshita, N. Kopidakis, K. Bothe, G. Siefert, X. Hao, *Prog. Photovolt.: Res. Appl.* **31** No 7, 651 (2023).
- D. Rached, H.M. Yssaad, W.L. Rahal, *J. Nano- Electron. Phys.* **10** No 5, 05012 (2018).
- H.S. Jung, N.G. Park, *Small* **11** No 1, 10 (2015).
- Y. Rong, Y. Hu, A. Mei, H. Tan, M.I. Saidaminov, S.I. Seok, M.D. McGehee, E.H. Sargent, H. Han, *Science* **361**, 6408 (2018).
- J. Gulomov, O. Accouche, R. Aliev, B. Neji, R. Ghandour, I. Gulomova, M. Azab, *Nanomaterials* **12** No 15, 2692 (2022).
- D. Wang, M. Wright, N.K. Elumalai, A. Uddin, *Sol. Energy Mater. Sol. Cells* **147**, 255 (2016).
- J. Gulomov, O. Accouche, R. Aliev, M. Azab, I. Gulomova, *Computers, Materials & Continua* **74** No 1, 575 (2022).
- L.C. Hirst, N.J. Ekins-Daukes, *Prog. Photovolt.: Res. Appl.* **19** No 3, 286 (2011).
- S.C. Baker-Finch, K.R. McIntosh, *Prog. Photovolt.: Res. Appl.* **19** No 4, 406 (2011).
- M. Hebali, M. Bennaoum, H.A. Azzeddine, B. Ibari, A. Maachou, D. Chalabi, *J. Nano- Electron. Phys.* **15** No 1, 01023 (2023).
- C.H. Seaman, *Sol. Energy* **29** No 4, 291 (1982).
- K. Liao, J. Chen, L. Xia, S. Zhong, X. Luo, *Opt Mater* **109**, 110318 (2020).
- J. Gulomov, R. Aliev, B. Urmanov, *J. Surf. Investig* **16** No 3, 416 (2022).
- T.K. Todorov, D.M. Bishop, Y.S. Lee, *Sol. Energy Mater. Sol. Cells* **180**, 350 (2018).
- A. De Vos, H. Pauwels, *Applied Physics* **25** No 2, 119 (1981).
- J. Gulomov, O. Accouche, *IEEE Access* **10**, 119558 (2022).
- J. Gulomov, R. Aliev, *J. Nano- Electron. Phys.* **13** No 4, 04033 (2021).
- I.P. Buryk, L.V. Odnodvoret, Ya.V. Khyzhnya, *J. Nano- Electron. Phys.* **13** No 1, 01012 (2021).
- B. Zaidi, M.S. Ullah, S. Zahra, S. Gagui, C. Shekhar, *J. Nano- Electron. Phys.* **13** No 5, 05016 (2021).
- J. Siecker, K. Kusakana, B.P. Numbi, *Renew. Sustain. Energy Rev.* **79**, 192 (2017).
- H.Z. Cummins, N. Knable, Y. Yeh, *Phys Rev Lett* **12** No 6, 150 (1964).
- M. Zebach, A. Hemmani, H. Khachab, *J. Nano- Electron. Phys.* **15** No 6, 06005 (2023).
- J. Gulomov, O. Accouche, B. Neji, J. Ziyotdinov, *IEEE Access* **11**, 102140 (2023).
- Y. Chung, N. Dagli, *IEEE J Quantum Electron* **26** No 8, 1335 (1990).
- K.H. Prykhodko, O.V. Botsula, *J. Nano- Electron. Phys.* **15** No 6, 06019 (2023).
- D. Yevick, T. Frieze, F. Schmidt, *J Comput Phys.* **168** No 2, 433 (2001).
- W. Hackbusch, *Poisson Equation* (Berlin: Springer publisher, 2017).
- D.H. Doan, A. Glitzky, M. Liero, *Zeitschrift fur Angewandte Mathematik und Physik* **70** No 2, 1 (2019).
- A. Schenk, *Solid State Electron* **35** No 11, 1585 (1992).
- M.J. Kerr, A. Cuevas, *J. Appl. Phys.* **91** No 4, 2473 (2002).
- N. Shahverdi, M. Yaghoubi, M. Goodarzi, A. Soleamani, *Sol. Energy* **189**, 111 (2019).
- L. Guan, G. Shen, Y. Liang, F. Tan, X. Xu, X. Tan, X. Li, *Opt. Laser Technol.* **120**, 105700 (2019).
- J. Gulomov, R. Aliev, *J. Nano- Electron. Phys.* **13** No 6, 06036 (2021).
- Z. Mrazkova, I.P. Sobkowicz, M. Foldyna, K. Postava, I. Florea, J. Pištora, P.R. Cabarrocas, *Prog. Photovolt.: Res. Appl.* **26** No 6, 369 (2018).
- S.C. Baker-Finch, K.R. McIntosh, *Prog. Photovolt.: Res. Appl.* **21** No 5, 960 (2013).
- H. Ohtsuka, M. Sakamoto, K. Tsutsui, Y. Yazawa, *Prog. Photovolt* **8** No 4, 385 (2000).
- S. Pal, A. Reinders, R. Saive, *IEEE J. Photovolt.* **10** No 6, 1803 (2020).

Текстуровані двосторонні кремнієві сонячні елементи за різних умов освітлення

R. Aliev¹, M. Komilov¹, N. Mirzaalimov¹, A. Mirzaalimov², S. Alive³, I. Gulomova¹, J. Gulomov²¹ Andijan State University, 170100 Andijan, Uzbekistan² Andijan State Pedagogical Institute, 170100 Andijan, Uzbekistan³ Andijan Machine Building Institute, 170100 Andijan, Uzbekistan

У сонячний день передня сторона двосторонніх сонячних елементів освітлюється прямим, а задня сторона – розсіяним світлом. Тому важливо вивчити вплив дифузії та прямого світла на двосторонній сонячний елемент. У цьому дослідженні шляхом моделювання було визначено вплив розсіяного та прямого світла та температури на текстурований двосторонній сонячний елемент. Відповідно до отриманих результатів, оптимальне значення кута бази текстури для двосторонньої кремнієвої сонячної батареї становить 580. У похмурий день, при розсіяному освітленні з обох сторін, площинні та оптимально текстуровані сонячні батареї мають ККД 13,14 % і 16,03 % і струм короткого замикання 4,34 мА/см² і 5,49 мА/см². Струм короткого замикання становить 2,28 мА/см² і 2,88 мА/см², коли розсіяним світлом освітлена лише лицьова сторона. У сонячний день, коли пряме світло падає на лицьову сторону, а розсіяне – на тильну, струм короткого замикання планарної та оптимально текстурованої сонячної батареї становить 27,79 мА/см² і 35,16 мА/см² відповідно. Струм короткого замикання становить 25,73 мА/см² і 32,65 мА/см², коли прямим світлом освітлена лише лицьова сторона.

Ключові слова: Кремнієвий сонячний елемент, Текстура, Дифузне світло, Пряме світло.